Recrystallization behavior of a Ni–20%Cr alloy subjected to severe plastic deformation

N. Dudova*, A. Belyakov, R. Kaibyshev

Belgorod State University, Belgorod 308015, Russia

Keywords:
Nanostructured alloys
Bulk deformation
Electron microscopy
Recrystallization
Grain growth

A B S T R A C T

The microstructure evolution in a Ni–20%Cr alloy was examined during deformation at large strains by high-pressure torsion (HPT) at ambient temperature with subsequent annealing. The structural changes during cold working to a strain of 2 were characterized by the development of a lamellar-type microstructure consisting of deformation twins and microbands. Further increase in the cold strain resulted in the evolution of nanoscale grains with a size of ~50 nm, and their volume fraction increased with strain, approaching 100% at $\varepsilon \sim 6$. The recrystallization processes under subsequent annealing were strongly dependent on the deformation structures. Discontinuous static recrystallization (DSRX) occurred in the alloy that was strained to $\varepsilon \leq 2$. This process occurred because of nucleation and the growth of new grains in the cold worked lamellar structure when the driving pressures for grain growth associated with stored dislocations and the grain boundary surface energy were approximately equal. The increasing fraction of nanoscale grains in the strain ranging from 3 to 4 led to the transition from DSRX to discontinuous grain coarsening (GC). Continuous GC occurred at $\varepsilon > 4$ because of the slow growth of the nanoscale grains. The transition from DSRX to GC took place when the driving pressure for grain growth associated with the grain boundary surface energy significantly exceeded the driving pressure attributed to stored dislocations.

1. Introduction

There is significant research interest in the utilization of severe plastic deformation (SPD) for the development of metals and alloys with ultra-fine grained (UFG) structures for structural applications [1,2]. Extensive nanoscale grain refinement leads to very high strength. However, such severely deformed metallic materials usually exhibit low ductility [1]. It has been shown that annealing metals and alloys that have been subjected to intense plastic strain might provide a unique combination of extremely high strength and good ductility [2]. Therefore, the annealing behavior of metals and alloys subjected to large-strain cold working are of specific interest [3–5]. However, their annealing behavior has not yet been fully explained. The properties of static recrystallization cannot be assumed to apply directly to metals and alloys subjected to SPD because severely deformed structures typically contain a high level of stored energy as a result of their high dislocation density and the large surface area of their deformation-induced boundaries [4–7].

Several studies have been carried out on the annealing behavior of severely strained nickel, copper, and aluminum alloys as well as stainless steel [1–6,8–19]. In those studies, the materials were almost all deformed to ultra-large strains with minimal overall change in the sample dimensions by the use of redundant deformation methods, such as equal channel angular pressing [1], high pressure torsion (HPT) [2], and multidirectional forging [11]. The recrystallization behavior of severely deformed materials was found to depend significantly on the material and process parameters. It is known [6,11] that recrystallization and grain growth may develop in two ways. If the development of an annealed microstructure occurs heterogeneously by nucleation and grain growth, it is described as occurring by discontinuous processes. The discontinuous recrystallization also includes discontinuous grain coarsening (DGC) [6]. Alternatively, recrystallization process may occur uniformly through the continuous increase of boundary misorientation and/or grain size. This process is described as continuous static recrystallization (CSRX) or continuous grain coarsening (CGC) [6]. Discontinuous processes lead to the formation of essentially non-uniform structures [3–5]. Only continuous processes form uniform UFG structures under annealing of alloys subjected to SPD [3,4,11,19], thereby producing exceptionally high mechanical properties. Thus, materials subjected to SPD may exhibit two distinctly different types of recrystallization behavior on subsequent annealing: homogeneous and heterogeneous. The character of the recrystallization behavior strongly depends on the deformation microstructure [6]. It has been suggested that

* Corresponding author.
E-mail address: dudova@bsu.edu.ru (N. Dudova).

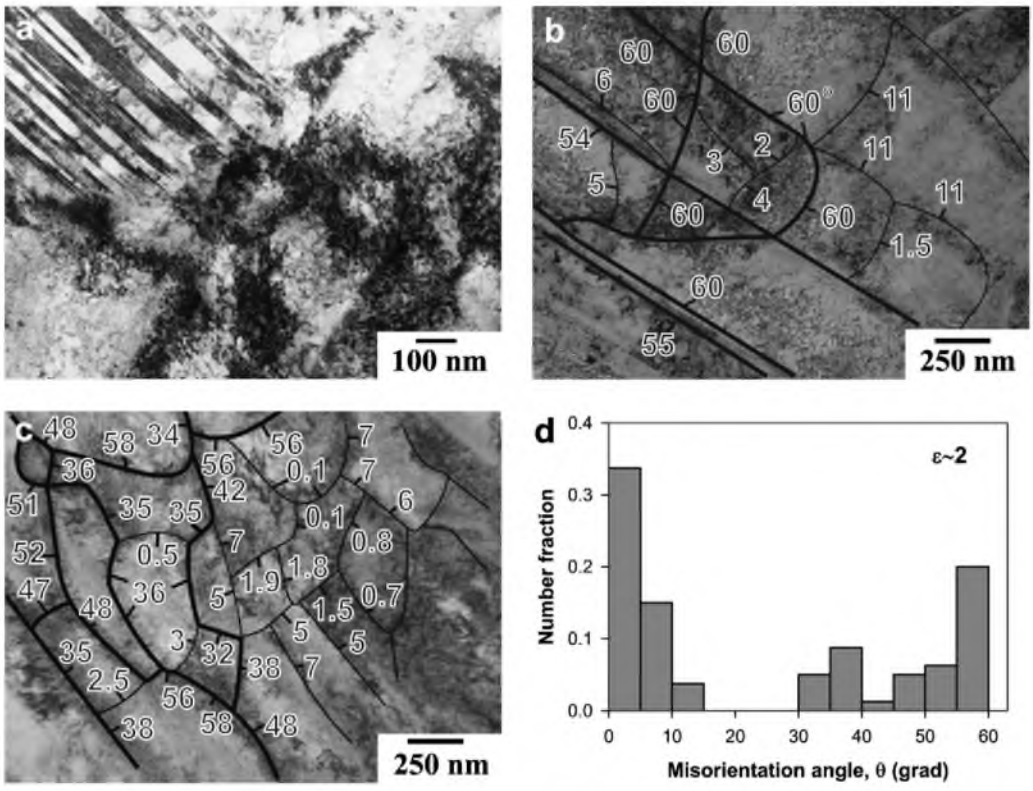

Fig. 1. Microstructure of Ni–20%Cr alloy strained to $\varepsilon \sim 2$ (a–c). Typical deformation twins with misorientation of 60° along the ⟨1 1 1⟩ direction (b). Substructure with boundaries closed to Σ5 boundaries with a misorientation of $\theta \sim 36.87°$ along the ⟨0 0 1⟩ direction (c). Distribution of (sub)boundary misorientation angle (d).

materials subjected to SPD are stable against DSRX and DGC if the fraction of high-angle boundaries (HABs) is larger than 0.64 [3]. This behavior has been observed in aluminum and aluminum alloys containing dispersions of secondary phases in a nearly pure aluminum matrix [3] when extrinsic grain boundary dislocations could be absorbed at ambient temperature. In contrast, pure nickel, in which the temperature of grain boundary dislocation absorption is ~350 °C [20], recrystallized discontinuously, although the fraction of HABs in the deformed state was as large as 0.68 [19]. The presence of impurities was shown to strongly affect the recrystallization behavior of severely deformed Ni because they reduced the mobility of HABs [19]. Thus, a large fraction of HABs (>0.64) is a prerequisite condition for the occurrence of CSRX/CGC during the static annealing of severely deformed materials [3,4,8]. However, this condition is not sufficient because of the effect of impurities and dispersoids on the recrystallization behavior [3,4]. In addition, the deformation structure, which strongly depends on the strain imposed [1,2,21–24], also strongly affects the recrystallization processes during annealing. For instance, deformation-induced lamellar structure usually exhibits instability during annealing [5] and undergoes DGC/DSRX. However, the effect of the deformation structure on the recrystallization mechanisms that operate during subsequent annealing has not been studied in sufficient detail [3–5].

The aim of the present study is to examine the transition from discontinuous to continuous annealing processes (recrystallization and grain coarsening) in a dilute Ni–20%Cr alloy that is strained to different degrees. To clarify the relationship between the deformation structure and the recrystallization behavior, the exact contribution of the driving forces for recrystallization and grain growth [6] that arise from the dislocation density and the boundary energy were evaluated. Ni–20%Cr alloy is a typical single-phase metallic material that has a low stacking fault energy (SFE) [25].

2. Experimental procedure

The Ni–20%Cr alloy having face centered cubic lattice examined in this study had a chemical composition of Ni–21%Cr–0.6% Si–0.3%Mn–0.75%Fe–0.31%Al–0.08%Ti–0.35%Cu–0.05%C (in wt%). A uniform structure with an average grain size of 100 μm was produced by annealing of a hot-rolled rod (Ø40 mm) at 1025 °C for 2 h, followed by air cooling. The HPT was carried out at room temperature using the procedure described in the overview [2] under an applied pressure (P) of 6 GPa. The specimens were prepared in the form of small disks with a diameter of ~10 mm and thickness of ~0.7 mm. The true strain (ε) imposed as a sum of the compression and torsion strains [2,24] was calculated as:

$$\varepsilon = \ln\left[1 + \left(\frac{\varphi r}{h}\right)^2\right]^{1/2} + \ln\frac{h_0}{h}, \quad (1)$$

where r is the distance from the sample center, $\varphi = 2\pi N$ (N is the number of whole revolutions), and h_0 and h are the initial and the final thicknesses of the specimen, respectively. All examinations of the microstructure and properties were carried out at a distance of ~2 mm from the center of each disk, $r = 2$ mm. The specimens were subjected to different strains, from ~1.5 to ~6.5, corresponding to 1/8 – 7 revolutions of a Bridgman anvil. An isochronal annealing of the strained specimens for 1 h was carried out at 500 °C in a vacuum furnace; a sample strained to $\varepsilon \sim 6.5$ was also annealed at 600 °C.

The microhardness measurements were carried out using a Wolpert 402MVD microhardness tester with a load of 200 g and a holding time of 20 s. The microstructure was examined with a JEM-2100 transmission electron microscope (TEM) operated at 200 kV. The specimens for structural examinations were prepared by electropolishing using an electrolyte of 10% perchloric acid in n-butanol at ambient temperature. The average grain size was measured by the linear intercept method, and the twin boundaries

were omitted from the measurements. The misorientations of the (sub)grain boundaries were studied by the conventional Kikuchi-line technique in TEM [26]. The accuracy of measurements was about 1° because of high dislocation densities evolved under cold deformation. The total number of boundaries analyzed in deformed samples was at least 80 at each strain. The dislocation densities were estimated by counting the individual dislocations in the grain/subgrain interiors per unit area on at least six arbitrarily selected typical TEM images for each data point. The dislocation densities and elastic distortions in the severely strained specimens were studied by high resolution TEM (HRTEM). The HRTEM study was carried out using an FEI Tecnai G2 F20F S-TWIN high resolution TEM with a field emission gun operated at 200 kV. Only free lattice dislocations were taken into account for calculation of the average dislocation density; the dislocations stored in low-angle boundaries (LABs) were omitted. The crystallographic features of the microstructure were determined using high-resolution electron back scattering diffraction (EBSD) with a Quanta 600FEG scanning electron microscope. The orientation image microscopy (OIM) image was obtained on the area of 30 μm × 30 μm with scanning pitch of 30 nm and then subjected to a cleanup procedure, setting the minimal confidence index to 0.07. On the misorientation map, white and black lines correspond to LABs and HABs with misorientations of $2 \le \theta < 15°$ and $15° \le \theta$, respectively. Differential scanning calorimetry was performed with an SDT Q600 (TA Instruments) device. Pure gold was used as an inert reference material, the sample weight was less than 0.1 g, and the experiments were carried out under an argon atmosphere.

3. Results

3.1. Deformation microstructures and strain hardening

The application of HPT to produce a strain of $\varepsilon \sim 2$ results in the development of a typical work-hardened microstructure containing dense dislocation pileups. The dislocation density drastically increases to $\rho = 8 \times 10^{14}\ m^{-2}$ (Fig. 1a), and the initial grains are subdivided into crystallites with a high aspect ratio. The misorientations of the longitudinal boundaries are significantly larger than those of the transverse boundaries. These lamellar-like (sub)structures are delimited by twin boundaries and/or low-to-moderate angle boundaries (Fig. 1b and c). The twin thickness ranges from 50 to 500 nm (Fig. 1b). Boundaries of the common type comprise a minor portion of the high-angle grain boundaries that are involved at this strain level. Three peaks can be clearly distinguished on the histogram of misorientation distribution (Fig. 1d); they are attributed to LABs, Σ3 coherent twin boundaries ($\theta \sim 60°$) and boundaries that are closed to Σ5 boundaries with a misorientation of $\theta \sim 36.87°$ along the ⟨0 0 1⟩ direction. The development of a lamellar microstructure with high dislocation density is accompanied by a notable strain hardening (Fig. 2) in which the microhardness increases by +260% from that of the initial state.

Upon further straining, the fractions of twin boundaries and LABs decrease (Figs. 3 and 4), while the dislocation density increases above $10^{15}\ m^{-2}$. Beyond $\varepsilon \sim 3$, the deformation (sub)grains with equiaxed shape are involved in some portions of the work-hardened substructure (Fig. 3a). These strain-induced crystallites are bounded partly by twin boundaries but mostly by HABs of the common type (Fig. 3a and b). Significantly lower fractions of LABs and twin boundaries were found compared with the specimen that was strained to $\varepsilon \sim 2$. Two well-defined peaks corresponding to HABs of the common type with misorientations of approximately 20° and 45° are observed on the grain boundary misorientation distribution (Fig. 3b). It is worth noting that the formation of HABs with a misorientation of 20° has rarely

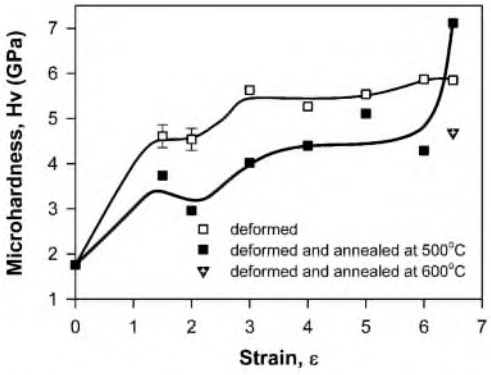

Fig. 2. Effect of strain and annealing on microhardness of a Ni–20%Cr alloy.

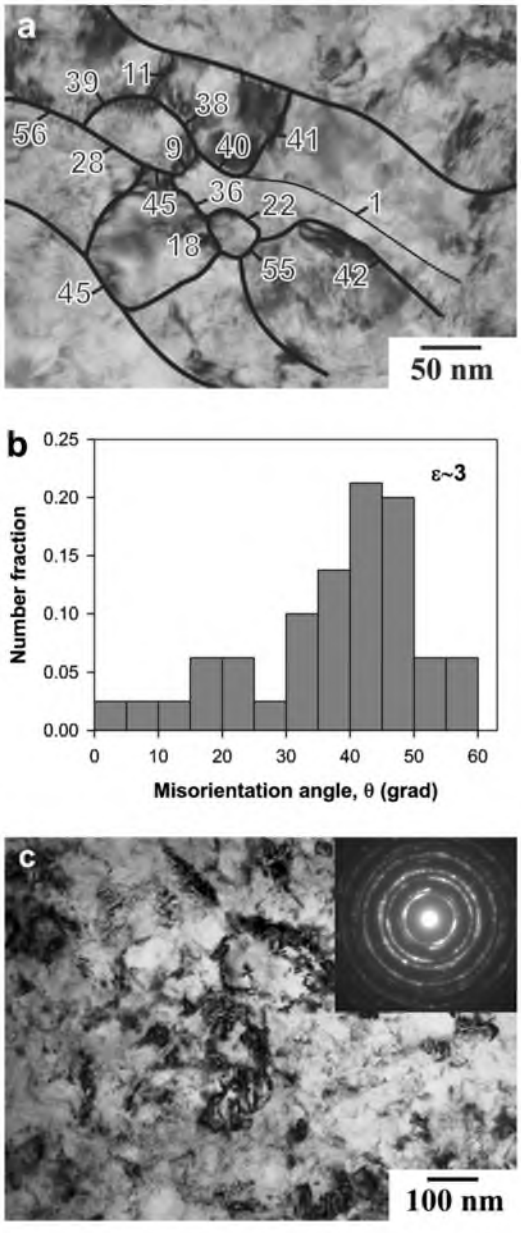

Fig. 3. Microstructure of a Ni–20%Cr alloy strained to $\varepsilon \sim 3$ (a) and distribution of (sub)boundary misorientation angle (b). Microstructure of a Ni–20%Cr alloy strained to $\varepsilon \sim 4$ (c).

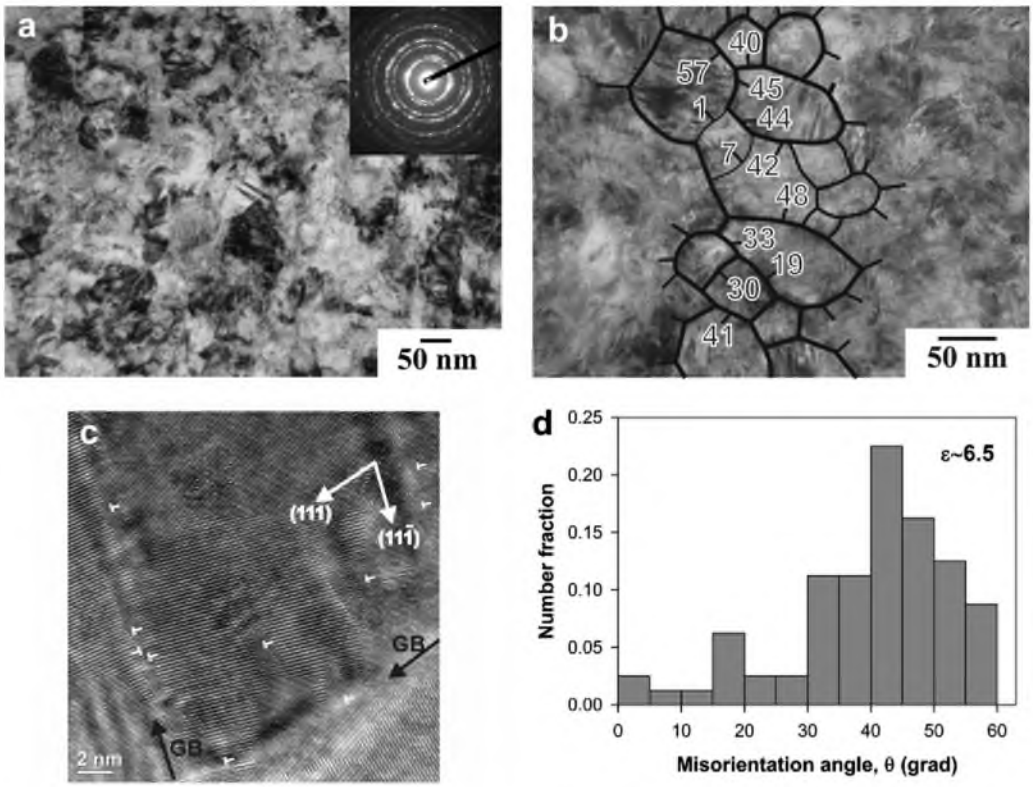

Fig. 4. Microstructure of a Ni–20%Cr alloy strained to $\varepsilon \sim 6.5$ (a–c). An HRTEM image of a grain containing dislocations at the grain boundaries (pointed by GB) and in grain interiors (c). Distribution of the (sub)boundary misorientation angle (d).

been observed in metallic materials processed by other deformation techniques. The microhardness increases by +24% as the strain increases from ~2 to ~3 (Fig. 2).

Beyond $\varepsilon \sim 4$, a mixed structure is observed that consists of nanoscale grains entirely delimited by common-type HABs and the work-hardened remainder of the original grains (Fig. 3c). The HABs do not exhibit a sharp contrast; their extinction contours are often very irregular because of the high density of extrinsic dislocations [27] that produce the long-range elastic stress fields of large magnitude [28,29]. There is no difference in the lattice dislocation density ($\rho = 3 \times 10^{15}\ m^{-2}$) between the nanoscale grains and the work-hardened (sub)structure. The high density of lattice dislocations also induces the large-magnitude long-range elastic stress fields. The development of nanoscale grains can be referred as low temperature dynamic recrystallization (LTDRX) [30]. However, this type of grain refinement is not the true recrystallization process because it does not restore the strained microstructure.

A uniform nanocrystalline structure with a crystallite size of approximately 50 nm evolves beyond $\varepsilon \sim 6.5$ (Fig. 4). The nanoscale crystallites that exhibit an equiaxed shape are entirely delimited by HABs (Fig. 4b). The grain boundary distribution at $\varepsilon \sim 6.5$ is similar to that at previous strain $\varepsilon \sim 3$; low fraction of LABs and two peaks corresponding to HABs of the common type with misorientations of approximately 17.5° and 42.5° are features of misorientation distribution of deformation-induced boundaries (Fig. 4d). An exceptionally high lattice dislocation density ($\rho = 7 \times 10^{15}\ m^{-2}$) is observed within the nanoscale grains. The non-equilibrium boundaries of nanoscale grains are characterized by the high density ($2 \times 10^{-8}\ m^{-1}$) of grain boundary dislocations (Fig. 4c). The exact identification of these dislocations is very difficult. It is most likely that these dislocations are lattice dislocations located at grain boundaries. However, their density, which is evaluated as a number of dislocations per boundary length, is very high and unambiguously can produce elastic strain of large magnitude. As a result, the development of such a nanocrystalline microstructure is accompanied by further strain hardening. The microhardness increases by +10% as the strain increases from ~3 to ~6.5.

The lattice dislocation density and the fraction of HABs are greater and crystallite size is smaller than the same structural parameters in Ni [2,19,21]. This difference in structural characteristics is attributed to the effects of SFE and solid solution on the structure evolution during SPD. As a result, the microhardness of the Ni–20%Cr alloy is higher than that of Ni subjected to the same strains [19,21,22].

3.2. Annealed microstructures and microhardness

Fig. 5a and b shows the annealed microstructures of the Ni–20%Cr alloy that was strained to $\varepsilon \sim 2$. The recrystallized fraction is ~50%, and the average size of the recrystallized grains is ~1.5 μm. Well-defined annealing twins are frequently involved in the new grains. The migration of HABs leads to a dramatic decrease in the lattice dislocation density, although small areas of dense dislocations remain within the interiors of the recrystallized grains. The deformation structure in the unrecrystallized portions remains almost unchanged, although there is an apparent increase in the lattice dislocation density to $\sim 2 \times 10^{15}\ m^{-2}$, and new grains have formed within the deformation structure. The (sub)grains that have an equiaxed shape and are bounded partly by LABs and partly by HABs of the common type can be observed in the unrecrystallized portions (Fig. 5b). These (sub)grains represent small volumes of relatively perfect material with a reduced dislocation density ($\rho \sim 4 \times 10^{13}\ m^{-2}$) and can be considered to be the recrystallization nuclei. No migration of twin boundaries was found. This lack of migration is associated with a low energy and an exceptionally low mobility of the Σ3 coherent twin boundaries [31–33].

Annealing after straining to $\varepsilon \sim 3$ also leads to the formation of a partially recrystallized structure (Fig. 5c–f) but with an increased

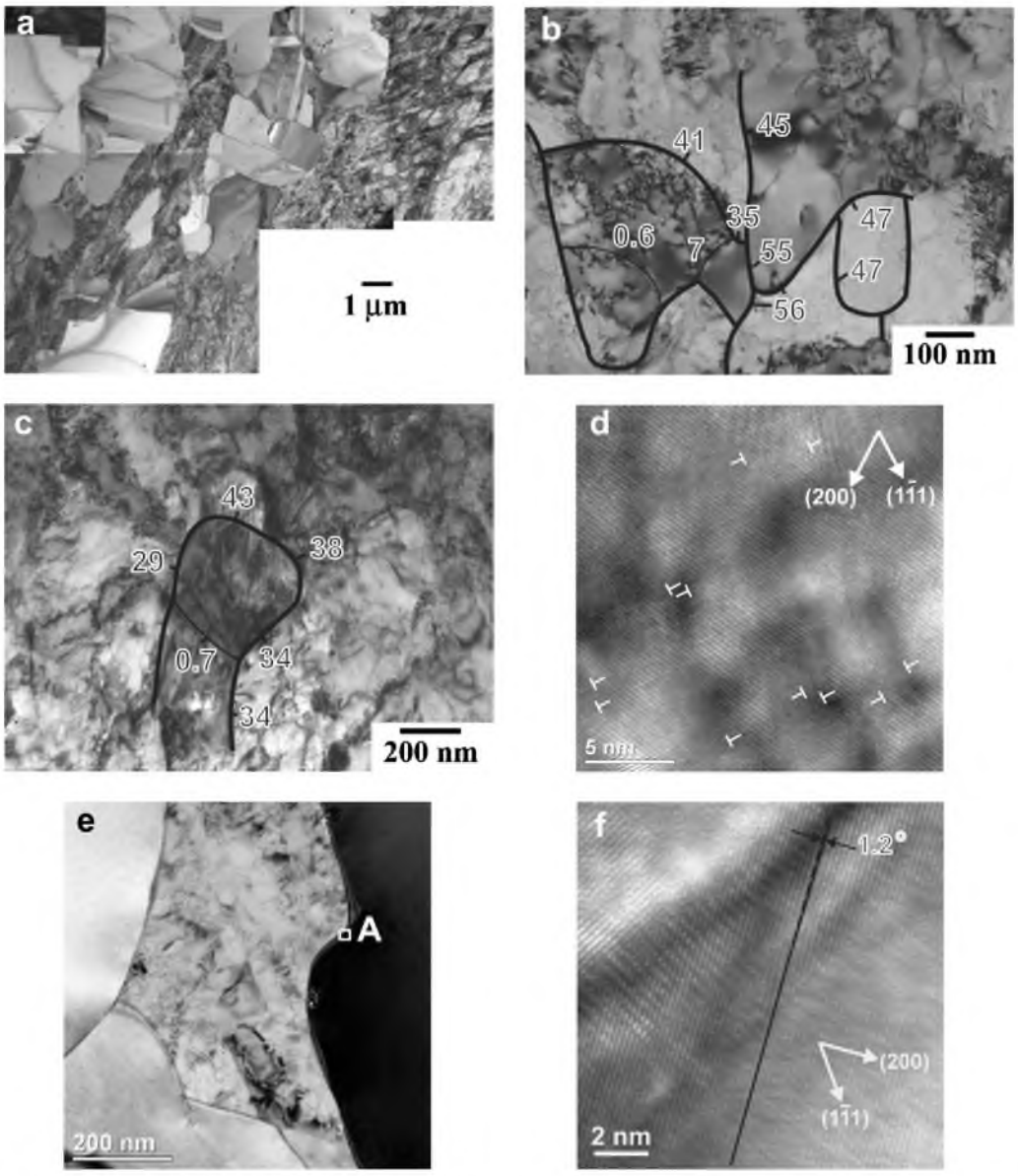

Fig. 5. Microstructure of a Ni–20%Cr alloy strained to $\varepsilon \sim 2$ (a and b) and $\varepsilon \sim 3$ (c–f) after annealing at 500 °C for 1 h. HRTEM images of (d) an unrecrystallized grain containing high dislocation density; (e and f) the boundary between unrecrystallized and recrystallized grains (within white rectangle A) with distortion of the lattice plane in the recrystallized grain near the boundary.

recrystallized fraction of ~70% and an average recrystallized grain size of ~0.9 μm. The recrystallization nuclei that are entirely delimited by HABs are the crystallites with a high dislocation density (Fig. 5c). A very high dislocation density of $\sim 2.3 \times 10^{16}\ m^{-2}$ can be found in some portions of the deformation structure (Fig. 5d). The internal stress, τ, attributed to this dislocation density, ρ, is evaluated by a method reported elsewhere [6,34] as:

$$\tau = 0.5 \rho G b^2, \tag{2}$$

where G is the shear modulus and b is the Burgers vector, $b = 2.5 \times 10^{-10}$ m. The internal stress, τ, was found to be $\sim 7.2 \times 10^{-4} G$. Some portions of the recrystallized grains near the boundaries between new grains and the work-hardened structure are characterized by large elastic distortions. The lattice curvature α of 1.2° at a distance l of 4.5 nm from the grain boundary in Fig. 5f corresponds to a dislocation density of $1.9 \times 10^{16}\ m^{-2}$ ($\rho = \alpha/(bl)$ [6,34]) and an internal stress of $\sim 5.8 \times 10^{-4} G$.

Static annealing of the specimen strained to $\varepsilon \sim 4$ leads to the formation of a fully recrystallized structure (Fig. 6a). The recrystallized microstructure, however, is not uniform. A bimodal distribution of the grain size (Fig. 6b) develops; the recrystallized grains with an average size of ~0.4 μm are surrounded by much finer grains with an average size of ~100 nm. This development suggests the occurrence of DGC. Annealing twins are frequently observed in recrystallized grains. Both the fine and coarse recrystallized grains are characterized by a low dislocation density of $\rho \sim 7 \times 10^{13}\ m^{-2}$. The boundaries of these grains exhibit well-defined extinction fringes, indicating their equilibrium state.

An annealed microstructure that consists of two structural components evolves in the specimen strained to $\varepsilon \sim 5$ (Fig. 7a). The first component consists of true recrystallized grains with an average size of ~0.25 μm. These grains contain a moderate dislocation density ($\rho \sim 1 \times 10^{14}\ m^{-2}$), and their boundaries exhibit clear extinction contours. The second component comprises nanoscale grains containing a high dislocation density. Their average size is

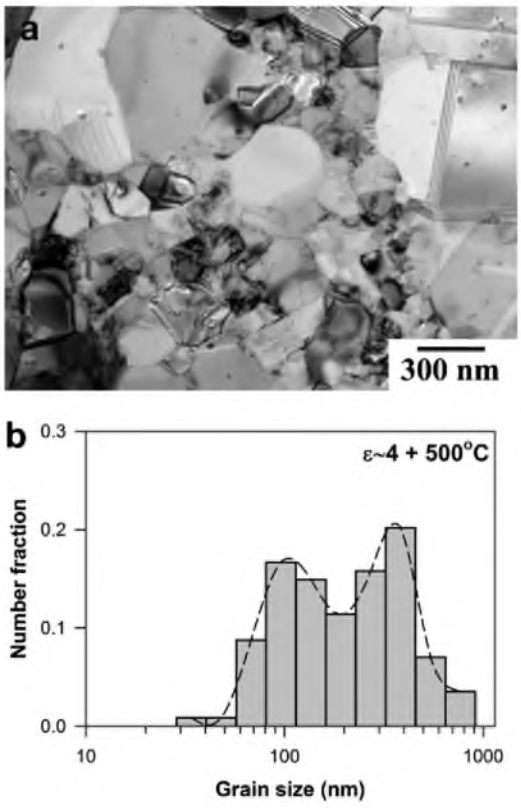

Fig. 6. Microstructure of a Ni–20%Cr alloy strained to $\varepsilon \sim 4$ and annealed at 500 °C for 1 h (a) and the corresponding grain size distribution (b).

~60 nm, and the boundaries exhibit a specific diffusive contrast that indicates a high density of grain boundary dislocations [35]. In the specimen strained to $\varepsilon \sim 6.5$, the volume fraction of nanoscale grains with a size of ~60 nm comprises ~1 (Fig. 7b). The single peak of the grain size distribution suggests the continuous mechanism for grain evolution, i.e., CGC (Fig. 7e). These grains contain a moderate dislocation density of $\rho \sim 4 \times 10^{14}\,m^{-2}$ (Fig. 7b), and the grain boundaries are not fully recovered. The elastic distortion of 0.5° at a distance of 4.5 nm from the boundary in Fig. 7d corresponds to a dislocation density of $7.8 \times 10^{15}\,m^{-2}$ and an internal stress of $\sim 3.4 \times 10^{-4}G$. Annealing of the specimen strained to $\varepsilon \sim 6.5$ results in a +12% increase in the microhardness compared to the deformed material; this result contrasts with that of the lower-strain samples, in which annealing led to softening (Fig. 2).

Isochronal annealing of the specimen strained to $\varepsilon \sim 6.5$ at 600 °C leads to the formation of a uniform recrystallized structure with an average grain size of ~160 nm (Fig. 8a). The misorientation distribution shows two well-defined peaks at small angles and large angle corresponding to Σ3 twin boundaries (Fig. 8b). A moderate dislocation density ($\rho \sim 4 \times 10^{14}\,m^{-2}$) remains in several grains (Fig. 8c), although most of grains contain a low dislocation density ($\rho \sim 3 \times 10^{13}\,m^{-2}$). Increasing the annealing temperature promotes the release of the elastic distortion that is attributed to a high density of grain boundary dislocations; as a result, the internal stress decreases to less than $\sim 0.1 \times 10^{-4}G$. Consequently, a 35% decrease in microhardness takes place as the temperature of isochronal annealing decreases from 500 to 600 °C (Fig. 2).

3.3. Differential scanning calorimetry

Fig. 9 shows the differential scanning calorimetry (DSC) curves for the specimens deformed to strains of ~2, ~4 and ~6.5. A DSC curve for a Ni–20%Cr sample that was water quenched after solution treatment is also included for comparison. The exothermic peaks near ~530 °C are located at nearly the same temperature for all states, indicating the presence of short-range ordering (SRO) in the alloy [36]. Exothermic peaks at exactly ~620 °C are observed for the samples strained to $\varepsilon \geq 4$; these peaks may be a result of the rapid recrystallization process.

Thus, DSC analysis shows that the ordering transformation of the deformed alloy occurs in the temperature interval of 450–600 °C, in agreement with previously published data [36]. Extraordinary hardening after annealing of severely deformed (~6.5) material at 500 °C may be a result of SRO in the Ni–20%Cr alloy in the temperature interval of 400–600 °C [37].

4. Discussion

Examination of the experimental results shows that three types of deformation structures evolve, depending on the strain imposed on the Ni–20%Cr alloy. The formation of these three different types of deformation structures leads to the operation of three different recrystallization mechanisms during the subsequent annealing. The density and structure of the HABs and the driving pressures for recrystallization and grain growth were shown to be of particular significance for determination of the recrystallization process (continuous or discontinuous) during annealing [3,4,6].

4.1. The deformed state

The microstructure evolution during SPD of Ni–20%Cr is typical for materials with low SFE [38] and quite different from that of materials with high SFE [2,5,10,12–15,17–19,39–41]. The main difference in the microstructural evolution between these two types of materials is that no dynamic equilibrium between dislocation generation and annihilation is attained in the Ni–20%Cr at any strain. As a result, the lattice dislocation density increases and the crystallite size decreases with strain, leading to a progressive increase of the microhardness over the entire strain interval. In addition, a well-defined transition from the lamellar (sub)structure (which is a result of nano-twinning and the alignment of deformation-induced boundaries and initial HABs with the plastic flow direction) to equiaxed grains takes place with increasing strain. Three different types of deformation structures could be distinguished:

(i) At $\varepsilon \leq 2$, a lamellar-like deformation (sub)structure with dense dislocation pile-ups evolves. Deformation twins and planar crystallites that are delimited by low-to-moderate angle boundaries comprise the lamellar structure.

(ii) In the strain interval of $2 < \varepsilon \leq 4$, the deformation structure tends to be uniform. The lamellar structure transforms into grains with an equiaxed shape because of the formation of transverse deformation-induced boundaries. These boundaries evolve as dislocation subboundaries, followed by an increase in their misorientation during SPD by trapping of glide dislocations [39]. As a result, dislocation LABs are converted to HABs that contain a high density of extrinsic boundary dislocations.

(iii) At $\varepsilon > 4$, the volume fraction of equiaxed grains increases with strain, leading to a uniform nanocrystalline structure at $\varepsilon \sim 6.5$. In the strain interval $4 < \varepsilon \leq 6$, the deformation structure consists of nanoscale grains and work-hardened areas with a high density of lattice dislocations. The density of the lattice dislocations tends to increase, while the mean crystallite size decreases with the application of strain. All deformation-induced HABs are non-equilibrium because of the high density of extrinsic dislocations.

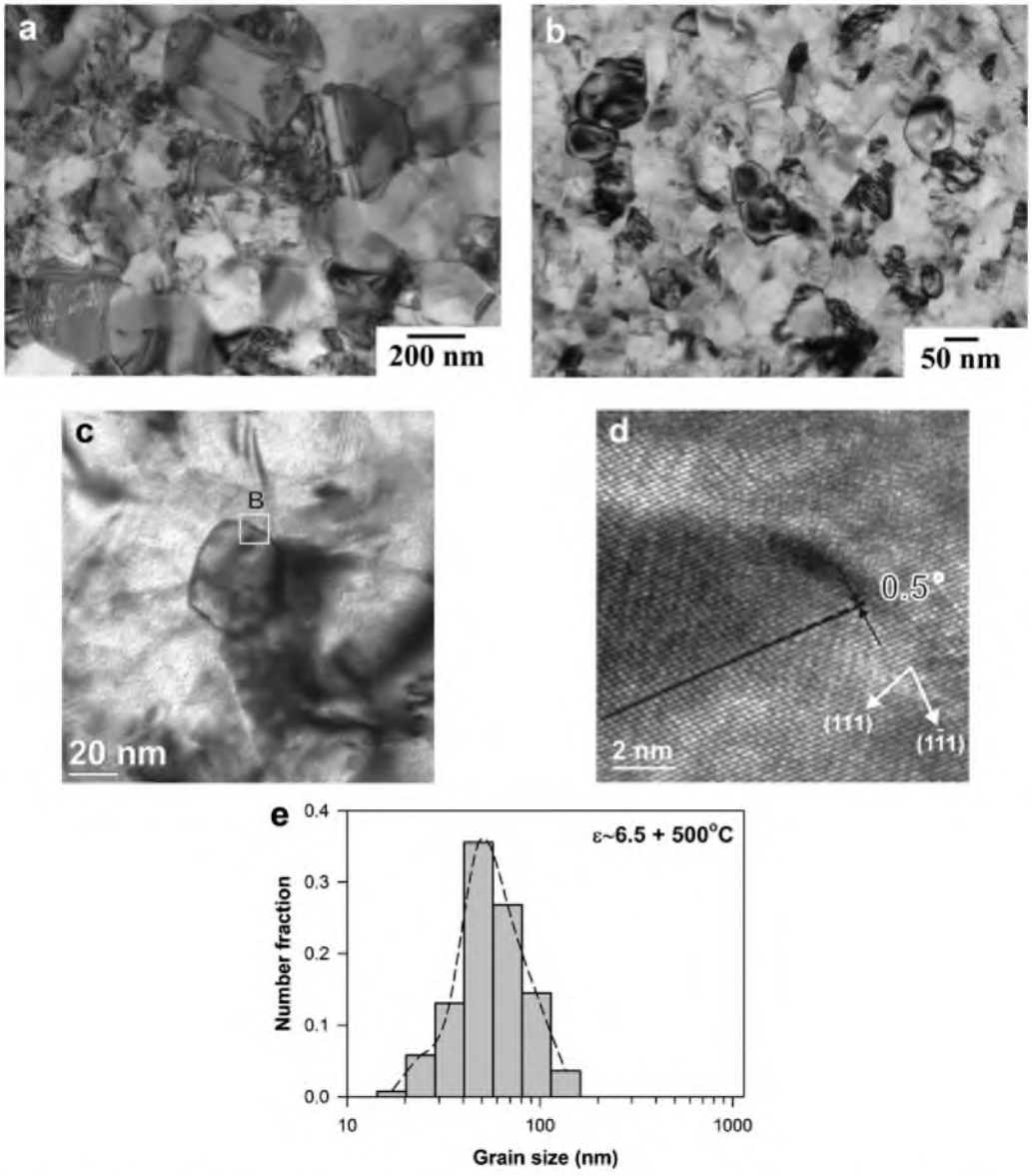

Fig. 7. Microstructure of a Ni–20%Cr alloy strained to $\varepsilon \sim 5$ (a) and $\varepsilon \sim 6.5$ (b–d) after annealing at 500 °C for 1 h. HRTEM images of the boundary of recrystallized grain (within white square B) with distortion of lattice plane in recrystallized grain near the boundary. (e) Grain size distribution of Ni–20%Cr alloy deformed to $\varepsilon \sim 6.5$ and annealed at 500 °C for 1 h.

The annealing behavior depends on the stored energy, which is associated with the deformation microstructures. In the present study, the driving pressures for recrystallization and the grain growth were calculated as stored energies associated with free lattice dislocations (P_1) and the surface energy of HABs (P_2). Because the surface energies of Σ5 boundaries and HABs of the common type are nearly equal [31], the Σ5 boundaries were treated as ordinary HABs. The coherent Σ3 twin boundaries were omitted because their energy is negligibly small [31–33].

The driving pressure due to stored dislocations (P_1) was determined to be [6]:

$$P_1 \sim 0.5\rho G b^2, \tag{3}$$

where ρ is the dislocation density, G is the shear modulus, and b is the Burgers vector. By taking $G = 83{,}100$ MPa, $b = 2.5 \times 10^{-10}$ m, and a dislocation density between 8×10^{14} and 7×10^{15} m^{-2}, P_1 is found to be between 2 MPa and 18 MPa.

The driving pressure due to the energy of high angle boundaries (P_2) was evaluated by [6]:

$$P_2 \sim \frac{2\gamma}{D} F_{\mathrm{HAB}}, \tag{4}$$

where γ is the boundary energy, D is the (sub)grain size, and F_{HAB} is the fraction of high angle boundaries. We used $\gamma = 1.25$ J/m^2 for Ni [31–33]. The evaluated driving pressures are presented in Table 1 along with the structural parameters used in the calculations.

The three types of deformation structure are distinguished by their P_2/P_1 ratios. Both types of driving pressures, P_1 and P_2, increase with increasing strain. However, the rate at which P_2 increases is significantly higher than that for P_1. At $\varepsilon \sim 2$, the driving pressures attributed to the dislocation structure and boundary energy are nearly equal. At $\varepsilon \geq 4$, $P_2/P_1 \sim 3$; the stored energy from the dislocation structure increases by a factor of 4 as the strain increases from ~2 to ~4, while P_2 increases by a factor of 13 because of the progressive increase of the density of deformation-induced boundaries and the transformation of low-energy LABs [31–33] to

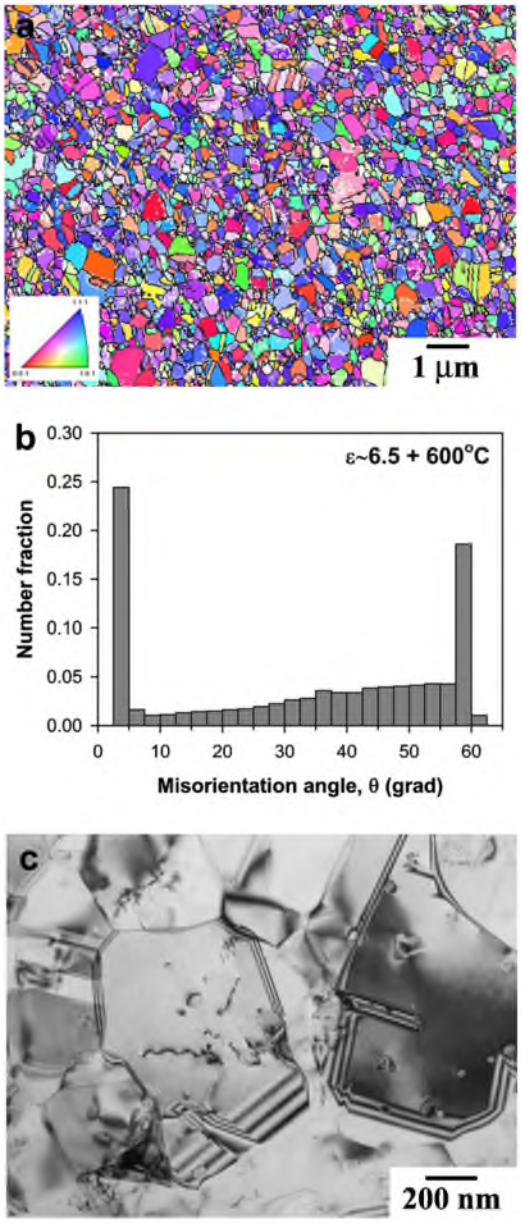

Fig. 8. Microstructure of a Ni–20%Cr alloy strained to $\varepsilon \sim 6.5$ and annealed at 600 °C for 1 h. (a) Typical OIM picture; white and black lines correspond to subgrain/grain boundaries with misorientations of $2^\circ \le \theta < 15^\circ$ and $15^\circ \le \theta$, respectively; (b) misorientation distribution of (sub)grain boundaries; (c) TEM image of recrystallized grains.

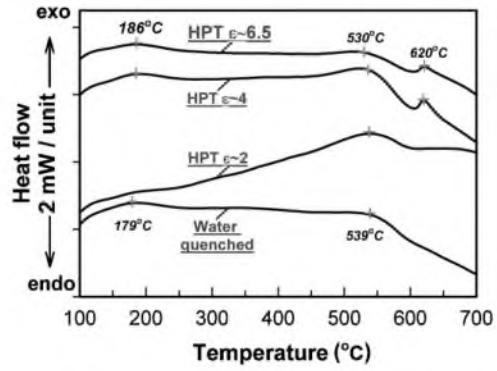

Fig. 9. DSC thermogram of Ni–20%Cr alloy heated at 20 °C/min in the water quenched condition after solution treatment at 1100 °C and after HPT to a strain of ~2, ~4 and ~6.5.

Table 1
Microstructural parameters and driving pressures for grain growth in the deformed Ni–20%Cr alloy.

	$\varepsilon \sim 2$	$\varepsilon \sim 4$	$\varepsilon \sim 6.5$
D_{grains} (nm)	500	100	50
ρ (m^{-2})	8×10^{14}	3×10^{15}	7×10^{15}
F_{HAB}	0.32	0.86	0.86
P_1 (MPa)	2	8	18
P_2 (MPa)	1.6	21	43
The main process	Discontinuous recrystallization	Discontinuous grain coarsening	Continuous grain coarsening

high-energy HABs. At $\varepsilon \sim 6.5$, the stored energy associated with P_2 (43 MPa) becomes extremely high and significantly exceeds P_1 (18 MPa) because of the large fraction of nanoscale grains with an average grain size of ~50 nm.

4.2. Recrystallization behavior

The effect of cold working on the subsequent annealing behavior of Ni–20%Cr is schematically represented in Fig. 10. Samples strained to $\varepsilon \le 2$ undergo DSRX on annealing. The DSRX occurs because of the growth of crystallites delimited by moderate-to-high angle boundaries through well-known mechanisms, which include the recovery-assisted evolution of dislocation-free recrystallization nuclei and their subsequent growth [6]. The migration of HABs eliminates the high dislocation density. However, despite a large driving pressure and the high mobility of the common-type grain boundaries [32], this growth occurs at a very low rate. It is apparent that the rate of DSRX is controlled by the ability of moving boundaries to absorb extrinsic boundary dislocations. Thus, if $P_1 \sim P_2$, DSRX occurs in the severely deformed Ni–20%Cr.

At higher strains, $P_2/P_1 \sim 3$, the number of recrystallization nuclei rapidly increases with strain. It should be noted that two different types of nuclei evolve. The first type originates from the lamellar grain structure, as described above. Their growth occurs discontinuously, i.e., the recrystallization nuclei grow by consuming their work-hardened surroundings. The second type of nucleus is attributed to nanoscale crystallites that evolve during HPT. The rapid transformation of deformation crystallites into recrystallization nuclei instantaneously results in a number of new fine grains. Because of the high density of these grains, their growth is limited, and their size is almost the same as the size of the preceding deformation crystallites. Therefore, DGC resulting in a bimodal grain size distribution is the main recrystallization process in the samples of Ni–20%Cr alloy that are subjected to SPD with strains ranging from 3 to 4. Similar behavior has been reported for pure Ni that was cold

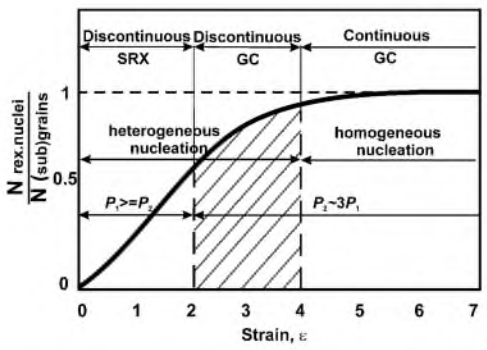

Fig. 10. Schematic presentation for variation of structural mechanisms responsible for new grain development during annealing of cold-worked Ni–20%Cr alloy, where $N_{rex,nuclei}$ is the number of recrystallization nuclei and $N_{(sub)grains}$ is the number of subgrains.

worked to a maximum strain of ~4 [19], calculated in accordance with Eq. (1).

In severely deformed alloy ($\varepsilon > 4$), the nanoscale grains, which originate from the strain-induced nanocrystalline structure, undergo insignificant growth during annealing at 500 °C (Fig. 7), and CGC takes place. As a result, a homogenous structure with a grain size of 60 nm develops. The formation of this nanograined structure is accompanied by additional hardening as a result of short range ordering [37] and precipitation of very small carbides. The precipitation of dispersoids during annealing can contribute to the stability of the nanocrystalline structure by exerting Zener drag pressure [6]. An increase in the annealing temperature to 600 °C leads to a three-fold increase in the size of the nanoscale grains, but the uniformity of the recrystallized structure remains. Therefore, the transition from discontinuous to continuous grain coarsening takes place because of the substitution of the lamellar structure by nanoscale grains in the deformed state of the Ni–20%Cr.

Thus, annealing can produce a uniform structure in Ni–20%Cr alloy if the relatively homogeneous nanocrystalline structure was developed by previous SPD. Short-range ordering can provide additional strengthening of dilute alloys with deformation-induced UFG structure. An increase in the annealing temperature promotes the formation of the uniform UFG structure, which is free of long-range stress fields that originate from high density of extrinsic boundary dislocations [29]. A non-uniform structure results from the discontinuous growth of work-hardened lamellar-like structural components.

5. Conclusions

The deformation and recrystallization behavior of Ni–20%Cr alloy subjected to high-pressure torsion at strains ranging from 1.5 to 6.5 was studied. The main results can be summarized as follows:

1. The structural changes during cold working to a strain of 2 were characterized by the development of a lamellar-type microstructure consisting of deformation twins and microbands.
2. An increase in the cold strain resulted in the evolution of nanoscale grains with a size of ~50 nm, and their volume fraction increased with strain, approaching 100% as the strain approached ~6.
3. Discontinuous static recrystallization and continuous grain coarsening occur during the annealing of strained samples. The transition from discontinuous static recrystallization to continuous grain coarsening with increasing strain takes place in a gradual manner through the transient region of discontinuous grain coarsening.
4. Samples strained to $\varepsilon \leq 2$ undergo discontinuous static recrystallization during annealing because of their relatively small number of recrystallization grains, which nucleate within the work-hardened lamellar-like (sub)structure.
5. The annealed microstructure is characterized by a bimodal grain size distribution in samples strained to $2 < \varepsilon \leq 4$. The large grains originate from discontinuous grain coarsening within the work-hardened volumes of the lamellar-like (sub)structure, while fine grains result from deformation-induced equiaxed nanocrystallites.
6. In severely deformed ($\varepsilon > 4$) alloy, a uniform microstructure consisting of nanoscale grains results from continuous grain coarsening.

Acknowledgments

The financial support received from the Federal Agency for Science and Innovations, Russia, under grant no. 16.740.11.0323 is gratefully acknowledged. The authors are grateful to the personnel of the Joint Research Centre, Belgorod State University, for their assistance with instrumental analysis.

References

[1] R.Z. Valiev, T.G. Langdon, Prog. Mater. Sci. 51 (2006) 881–981.
[2] A.P. Zhilyaev, T.G. Langdon, Prog. Mater. Sci. 53 (2008) 893–979.
[3] H. Jazaeri, F.J. Humphreys, Acta Mater. 52 (2004) 3251–3262.
[4] M. Ferry, N.E. Hamilton, F.J. Humphreys, Acta Mater. 53 (2005) 1097–1109.
[5] G.H. Zahid, Y. Huang, P.B. Prangnell, Acta Mater. 57 (2009) 3509–3521.
[6] F.J. Humphreys, M. Hatherly, Recrystallization and Related Annealing Phenomena, Pergamon Press, UK, 2004.
[7] J.H. Driver, Scripta Mater. 51 (2004) 819–823.
[8] A. Oscarsson, H.-E. Ekstrom, B. Hutchinson, Mater. Sci. Forum 113–115 (1993) 177–178.
[9] H. Jiang, Y.T. Zhu, D.P. Butt, I.V. Alexandrov, T.C. Lowe, Mater. Sci. Eng. A 290 (2000) 128–138.
[10] S. Lee, A. Utsunomiya, H. Akamatsu, K. Neishi, M. Furukawa, Z. Horita, T.G. Langdon, Acta Mater. 50 (2002) 553–564.
[11] A. Belyakov, T. Sakai, H. Miura, R. Kaibyshev, K. Tsuzaki, Acta Mater. 50 (2002) 1547–1557.
[12] D.G. Morris, M.A. Munoz-Morris, Acta Mater. 50 (2002) 4047–4060.
[13] E. Schafler, R. Pippan, Mater. Sci. Eng. A 387–389 (2004) 799–804.
[14] C.Y. Yu, P.L. Sun, P.W. Kao, C.P. Chang, Mater. Sci. Eng. A 366 (2004) 310–317.
[15] Q. Xing, X. Huang, N. Hansen, Metall. Mater. Trans. 37A (2006) 1311–1322.
[16] X. Molodova, G. Gottstein, M. Winning, R.J. Hellmig, Mater. Sci. Eng. A 460–461 (2007) 204–213.
[17] N. Hansen, X. Huang, M.G. Møller, A. Godfrey, J. Mater. Sci. 43 (2008) 6254–6259.
[18] W.Q. Cao, A. Godfrey, N. Hansen, Q. Liu, Metall. Mater. Trans. 40A (2009) 204–214.
[19] H.W. Zhang, X. Huang, R. Pippan, N. Hansen, Acta Mater. 58 (2010) 1698–1707.
[20] M.F. Imayev, Phys. Met. Metallogr. 64 (1987) 824–826.
[21] A.P. Zhilyaev, G.V. Nurislamova, B.-K. Kim, M.D. Baro, J.A. Szpunar, T.G. Langdon, Acta Mater. 51 (2003) 753–765.
[22] A.P. Zhilyaev, A.A. Gimazov, E.P. Soshnikova, A. Revesz, T.G. Langdon, Mater. Sci. Eng. A 489 (2008) 207–212.
[23] N. Dudova, R. Kaibyshev, V. Valitov, in: Y.T. Zhu, T.G. Langdon, R.S. Mishra, S.L. Semiatin, M.J. Saran, T.C. Lowe (Eds.), Ultrafine Grained Materials II, The Minerals, Metals and Materials Society, Warrendale, PA, 2002, pp. 75–80.
[24] O.A. Kaibyshev, N.R. Dudova, V.A. Valitov, Phys. Met. Metallogr. 96 (2003) 48–54.
[25] B.A. Wilcox, A.H. Clauer, Metal Sci. J. 3 (1969) 26–33.
[26] G. Thomas, M.J. Goringe, Transmission Electron Microscopy of Materials, Wiley, New York, NY, 1979, pp. 112–124.
[27] M. Mabuchi, K. Ameyama, H. Iwasaki, K. Higashi, Acta Mater. 47 (1999) 2047–2057.
[28] A. Belyakov, T. Sakai, H. Miura, R. Kaibyshev, Scripta Mater. 42 (2000) 319–325.
[29] T. Shimokawa, T. Kinari, S. Shintaki, Phys. Rev. B 75 (2007) 144108.
[30] A. Galiyev, R. Kaibyshev, Mater. Trans. 42 (2001) 1190–1199.
[31] D.L. Olmsted, S.M. Foiles, E.A. Holm, Acta Mater. 57 (2009) 3694–3703.
[32] D.L. Olmsted, S.M. Foiles, E.A. Holm, Acta Mater. 57 (2009) 3704–3713.
[33] G.S. Rohrer, E.A. Holm, A.D. Rollett, S.M. Foiles, J. Li, D.L. Olmsted, Acta Mater. 58 (2010) 5063–5069.
[34] J.P. Hirth, J. Lothe, Theory of Dislocations, New York, McGraw-Hill, 1968.
[35] R.Z. Valiev, V.Yu. Gertsman, O.A. Kaibyshev, Phys. Stat. Sol. (a) 97 (1986) 11–56.
[36] E. Lang, V. Lupinc, A. Marucco, Mater. Sci. Eng. A 114 (1989) 147–157.
[37] N.R. Dudova, R.O. Kaibyshev, V.A. Valitov, Phys. Met. Metallogr. 108 (2009) 625–633.
[38] Z.J. Zhang, Q.Q. Duan, X.H. An, S.D. Wu, G. Yang, Z.F. Zhang, Mater. Sci. Eng. A 528 (2011) 4259–4267.
[39] D.A. Hughies, N. Hansen, Acta Mater. 48 (2000) 2985–3004.
[40] G. Winter, D.J. Jensen, N. Hansen, Acta Mater. 45 (1997) 3871–3886.
[41] H. Jazaeri, F.J. Humphreys, Acta Mater. 52 (2004) 3239–3250.